Anal. Chem. **2005,** *77,* 7976−7983

A Scalable Addressable Positive-Dielectrophoretic Cell-Sorting Array

Brian M. Taff and Joel Voldman*

Department of Electrical Engineering and Computer Science, Massachusetts Institute of Technology, 77 Massachusetts Avenue, Building 36-854, Cambridge, Massachusetts 02139

We present the first known implementation of a passive, scalable architecture for trapping, imaging, and sorting individual microparticles, including cells, using a positive dielectrophoretic (p-DEP) trapping array. Our array-based technology enables "active coverslips" where, when scaled, many individually held cells can be sorted based upon imaged spatial or temporally variant characteristics. Our design incorporates a unique "ring-dot" p-DEP trap geometry organized in a row/column array format. This trap design, implemented in a two-level metal process, provides strong and highly spatially localized holding fields enabling single-cell capture for all traps in the array. We release individual trapped microparticles during sorting using a passive transistor-independent approach where we electrically ground the row and column electrodes associated with specific traps in the array. The demand for chip-to-world electrical connections in our arrays scales proportionally with the square root of the number of traps in a given array, delivering a substantial improvement over prior designs. We demonstrate capture, holding, and release operations with both beads and cells in small arrays of this new architecture.

In the past 15 years or more, microfabricated array-based structures have seen widespread use in cell-based applications ranging from patterned neural networks[1,2] to coculture systems,[3−5] cell-based biosensors,[6−8] secretion measurement tools,[9,10] cellular force measurements,[11] drug delivery systems,[12,13] and even transfection platforms for monitoring gene expression.[14,15] On a most basic level, arrays present clean and simple methods for visualizing and indexing cells positioned within assayed populations.[16−18] In this form, they assign unique position-specific information to the assayed cells. Information about variations across collections of cells is also easily obtained using an array format as the heterogeneity of cells that are nominally phenotypically similar can be assessed when subjected to a single prescribed set of stimuli.[6,10,19] By managing the cells' position and environment, arrays often enhance the reliability and statistical significance of collected data through redundancy. In other words, multiple repeats of the same assay condition can be examined in unison. Furthermore, by assaying libraries of distinct mutants[14,15,20] or by examining arrays where different stimuli are directed to different subpopulations of phenotypically similar cells,[21−23] it is even feasible to simultaneously monitor large collections of distinct assay conditions.

Microfabricated arrays used in biological applications can be loosely classified into a few types. One is passive and simply serves to hold objects in specific locations. Such arrays generally operate either by presenting patterned adhesive regions[3,4] or by defining mechanical structures that serve as small containers to physically confine biomaterial to specified positions.[16,17] Others are globally active, enabling dynamic simultaneous control over all sites in the array. Arrays of this type include devices where the surface features[24,25] or even the trapping potential[26,27] of all sites in the

* To whom correspondence should be addressed. Email: voldman@mit.edu. Fax: 617-258-5846.

(1) Suzuki, I.; Sugio, Y.; Jimbo, Y.; Yasuda, K. *Lab Chip* **2005**, *5*, 241−247.
(2) Nam, Y.; Chang, J. C.; Wheeler, B. C.; Brewer, G. J. *IEEE Trans. Biomed. Eng.* **2004**, *51*, 158−165.
(3) Bhatia, S. N. B., U. J.; Yarmush, M. L.; Toner, M. *Biotechnol. Prog.* **1998**, *14*, 378−387.
(4) Folch, A., Toner, M. In *Annual Review of Biomedical Engineering*; Annual Reviews: Palo Alto, CA, 2000; Vol. 2, pp 227−256.
(5) Barron, J. A., Wu, P., Ladouceur, H. D., and Ringeisen, B. R. *Biomed. Microdevices* **2004**, *6*, 139−147.
(6) McFadden, P. *Science* **2002**, *297*, 2075−2076.
(7) Pancrazio, J. J.; Whelan, J. P.; Borkholder, D. A.; Ma, W.; Stenger, D. A. *Ann. Biomed. Eng.* **1999**, *27*, 697−711.
(8) Kovacs, G. T. A. *Proc. IEEE* **2003**, *91*, 915−929.
(9) Chen, P.; Xu, B.; Tokranova, N.; Feng, X.; Castracane, J.; Gillis, K. D. *Anal. Chem.* **2003**, *75*, 518−524.
(10) Isik, S.; Berdondini, L.; Oni, J.; Blochl, A.; Koudelka-Hep, M.; Schuhmann, W. *Biosens. Bioelectron.* **2005**, *20*, 1566−1572.
(11) Tan, J. L., Tien, J., Pirone, D. N., Gray, D. S., Bhadriraju, K., Chen, C. S. *Proc. Natl. Acad. Sci. U.S.A.* **2002**, *100*, 1484−1489.
(12) Peterman, M. C.; Mehenti, N. Z.; Bilbao, K. V.; Lee, C. J.; Leng, T.; Noolandi, J.; Bent, S. F.; Blumenkranz, M. S.; Fishman, H. A. *Artif. Organs* **2003**, *27*, 975−985.
(13) Shawgo, R. S.; Grayson, A. C. R.; Li, Y. W.; Cima, M. J. *Curr. Opin. Solid State Mater. Sci.* **2002**, *6*, 329−334.
(14) McKnight, T. E.; Melechko, A. V.; Hesnley, D. K.; Mann, D. G. J.; Griffin, G. D.; Simpson, M. L. *Nano Lett.* **2004**, *4*, 1213−1219.
(15) Ziauddin, J.; Sabatini, D. M. *Nature* **2001**, *411*, 107−110.
(16) Walt, D. R. *Curr. Opin. Chem. Biol.* **2002**, *6*, 689−695.
(17) Ostuni, E.; Chen, C. S.; Ingber, D. E.; Whitesides, G. M. *Langmuir* **2001**, *17*, 2828−2834.
(18) Folch, A.; Jo, B.-H.; Hurtado, B.-H.; Beebe, D. J.; Hurtado, O.; Toner, M. *J. Biomed. Mater. Res.* **2000**, *52*, 346−353.
(19) Chin, V. I.; Taupin, P.; Sanga, S.; Scheel, J.; Gage, F. H.; Bhatia, S. N. *Biotechnol. Bioeng.* **2004**, *88*, 399−415.
(20) Kapur, R., Giuliano, K. A., Campana, M., Adams, T., Olson, K., Jung, D., Mrksich, M., Vasudevan, C., and Taylor, D. L. *Biomed. Microdevices* **1999**, *2*, 99−109.
(21) Hung, P. J.; Lee, P. J.; Sabounchi, P.; Lin, R.; Lee, L. P. *Biotechnol. Bioeng.* **2005**, *89*, 1−8.
(22) Takayama, S., Ostuni, E., LeDuc, P., Naruse, K., Ingber, D., Whitesides, G. *Chem. Biol.* **2003**, *10*, 123−130.
(23) Thompson, D. M.; King, K. R.; Wieder, K. J.; Toner, M.; Yarmush, M. L.; Jayaraman, A. *Anal. Chem.* **2004**, *76*, 4098−4103.

10.1021/ac0513616 CCC: $30.25
Published on Web 11/15/2005

array can be switched from one state to another in a parallel fashion. Last, active addressable arrays present avenues for changing or mapping different conditions to specific sites.[28−30] The mechanisms for switching individual sites in this sort of array are often similar to those used in globally active arrays but modified to permit individual site control. In general, the intended application of a given array mandates its associated levels of functionality and complexity.

Placing cells in arrays requires various manipulation techniques. To date, most applications have incorporated physical, optical, or electrical forces either in isolation or in some appropriate combination. Examples of physical means for cell manipulation include microwell structures,[16,17,31] patch clamping devices,[32] controllable ciliary paddles,[33] micropatterned substrates,[2,18,19,24,34] and even microbubble generators.[35] In complementary fashion, optical tweezers have been used in studies assessing growth mechanisms in individual bone and cartilage cells[36] and optical lattices have been used to separate cell populations based upon size.[37] Electrical manipulation strategies generally rely upon dielectrophoresis (DEP).[26,27,38,39] This dependence has arisen largely because DEP capitalizes upon the intrinsic electric polarizability of cells as a means for exerting forces. DEP techniques have included field-flow fractionation for separations,[40,41] avenues for assessing cell viability,[42] methods for manipulating nanoliters of fluid,[43] manipulating submicrometer-scale particles,[44,45] two- and three-dimensional electrode structures for focusing or caging biomaterial,[27,30,46,47] and optically driven DEP for manipulating particles.[48]

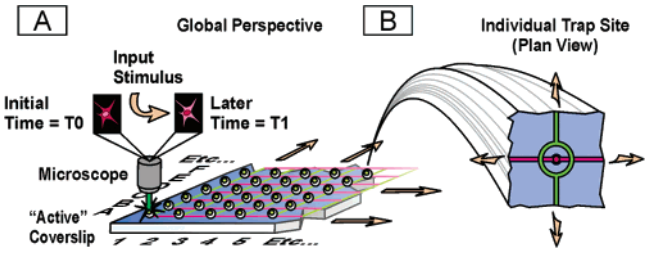

Figure 1. (A) Schematic outline of the overall functionality of the active coverslip. Individual cells are held in specified locations in the trapping array, interrogated using microscopy methods, and then sorted by grounding the associated row and column electrodes (shown in red and green, respectively). (B) Highlights an individual pixel within the holding array, displaying the unique, planar ring-dot-shaped p-DEP trap geometry.

Complementing the vast body of work developed for prior array-based microstructures, we present a DEP-based method for augmenting available active addressable arrays. We offer the first known implementation of a transistor-independent scalable architecture for trapping, imaging, and sorting many individual cells using a positive-dielectrophoretic (p-DEP) trapping array. The general architecture, outlined in Figure 1, provides a means for creating "active coverslips" that enable cell sorting based upon visually observed characteristics. We organize the DEP traps into a regular rectangular array. This format places cells in defined patterns within a microfluidic chamber where specific cells can be visually located and selectively released by deactivating the associated DEP traps. As opposed to our previous active addressable cell array,[30] which used one addressing electrode for each trap, here we use a row/column addressing scheme that is much more efficient.

Our approach moves beyond DEP trapping approaches that offer globally active control (e.g., all traps on or off) for all traps in the array,[26,27,45,46] while avoiding known challenges that limit existing active addressable approaches. Such existing active addressable approaches have used CMOS-based architectures with elaborate fabrication processes,[49] distinct electrical connections to each trap that pose heavy demands on chip-to-world connections upon scaling and limit the overall packing density of traps in a given array[30,50] or three-dimensional electrode geometries[39] that best suit individual cell translation rather than sorting. Contrasting many of these prior efforts, our active addressable technology provides an easily scaled method for trapping large collections of individual cells in prescribed locations and subsequently enabling the release of small numbers of specific cells from the held populations.

METHODS AND MATERIALS

Microfabrication. We fabricated our active coverslip devices using a two-level metal process on silicon substrates. An initial

(24) Jiang, X.; Ferrigno, R.; Mrksich, M.; Whitesides, G. M. *J. Am. Chem. Soc.* **2003**, *125*, 2366−2367.
(25) Hayward, R. C.; Saville, D. A.; Aksay, I. A. *Nature* **2000**, *404*, 56−59.
(26) Gray, D. S.; Tan, J. L.; Voldman, J.; Chen, C. S. *Biosens. Bioelectron.* **2004**, *19*, 771−780.
(27) Rosenthal, A.; Voldman, J. *Biophys. J.* **2005**, *88*, 2193−2205.
(28) Huang, Y.; Ewalt, K. L.; Tirado, M.; Haigis, R.; Forster, A.; Ackley, D.; Heller, M. J.; O'Connell, J. P.; Krihak, M. *Anal. Chem.* **2001**, *73*, 1549−1559.
(29) Heller, M. J.; Forster, A. H.; Tu, E. *Electrophoresis* **2000**, *21*, 157−164.
(30) Voldman, J.; Toner, M.; Gray, M. L.; Schmidt, M. A. *Anal. Chem.* **2002**, *74*, 3984−3990.
(31) Sato, K.; Kawamura, Y.; Tanaka, S.; Uchida, K.; Kohida, H. *Sens. Actuators, A* **1990**, *21−23*, 948−953.
(32) Khine, M.; Lau, A.; Ionescu-Zanetti, C.; Seo, J.; Lee, L. P. *Lab Chip* **2005**, *5*, 38−43.
(33) Suh, J. W.; Darling, R. B.; Bohringer, K.-F.; Donald, B. R.; Baltes, H.; Kovacs, G. T. A. *J. Microelectromech. Syst.* **1999**, *8*, 483−496.
(34) Revzin, A.; Tompkins, R. G.; Toner, M. *Langmuir* **2003**, *19*, 9855−9862.
(35) Maxwell, R. B.; Gerhardt, A. L.; Toner, M.; Gray, M. L.; Schmidt, M. A. *J. Microelectromech. Syst.* **2003**, *12*, 630−640.
(36) Walker, L. M.; Holm, A.; Cooling, L.; Maxwell, L.; Oberg, A.; Sundqvist, T.; El Haj, A. J. *FEBS Lett.* **1999**, *459*, 39−42.
(37) MacDonald, M. P.; Spalding, G. C.; Dholakia, K. *Nature* **2003**, *426*, 421−424.
(38) Fuhr, G.; Glasser, H.; Muller, T.; Schnelle, T. *Biochim. Biophys. Acta* **1994**, *1201*, 353−360.
(39) Suehiro, J.; Pethig, R. *J. Phys. D: Appl. Phys.* **1998**, 3298−3305.
(40) Wang, X.-B.; Vykoukal, J.; Becker, F. F.; Gascoyne, P. R. C. *Biophys. J.* **1998**, *74*, 2689−2701.
(41) Markx, G. H.; Pethig, R.; Rousselet, J. *J. Phys. D: Appl. Phys.* **1997**, *30*, 2470−2477.
(42) Goater, A. D.; Burt, J. P. H.; Pethig, R. *J. Phys. D: Appl. Phys.* **1997**, *30*, 65−69.
(43) Jones, T. B.; Gunji, M.; Washizu, M.; Feldman, M. J. *J. Appl. Phys.* **2001**, *89*, 1441−1448.
(44) Hughes, M. P.; Morgan, H. *J. Phys. D: Appl. Phys.* **1998**, *31*, 2205−2210.
(45) Muller, T.; Gerardino, A.; Schnelle, T.; Shirley, S. G.; Bordoni, F.; De Gasperis, G.; Leoni, R.; Fuhr, G. *J. Phys. D: Appl. Phys.* **1996**, *29*, 340−349.
(46) Schnelle, T.; Hagedorn, R.; Fuhr, G.; Fiedler, S.; Muller, T. *Biochim. Biophys. Acta* **1993**, *1157*, 127−140.
(47) Yu, C.; Vykoukal, J.; Vykoukal, D. M.; Schwartz, J. A.; Shi, L.; Gascoyne, P. R. C. *J. Microelectromech. Syst.* **2005**, *14*, 480−487.
(48) Chiou, P. Y.; Ohta, A. T.; Wu, M. C. *Nature* **2005**, *436*, 370−372.
(49) Manaresi, N.; Romani, A.; Medoro, G.; Altomare, L.; Leonardi, A.; Tartagni, M.; Guerrieri, R. *IEEE J. Solid-State Circuits* **2003**, *38*, 2297−2305.
(50) Cheng, J.; Sheldon, E. L.; Wu, L.; Heller, M. J.; O'Connell, J. P. *Anal. Chem.* **1998**, *70*, 2321−2326.

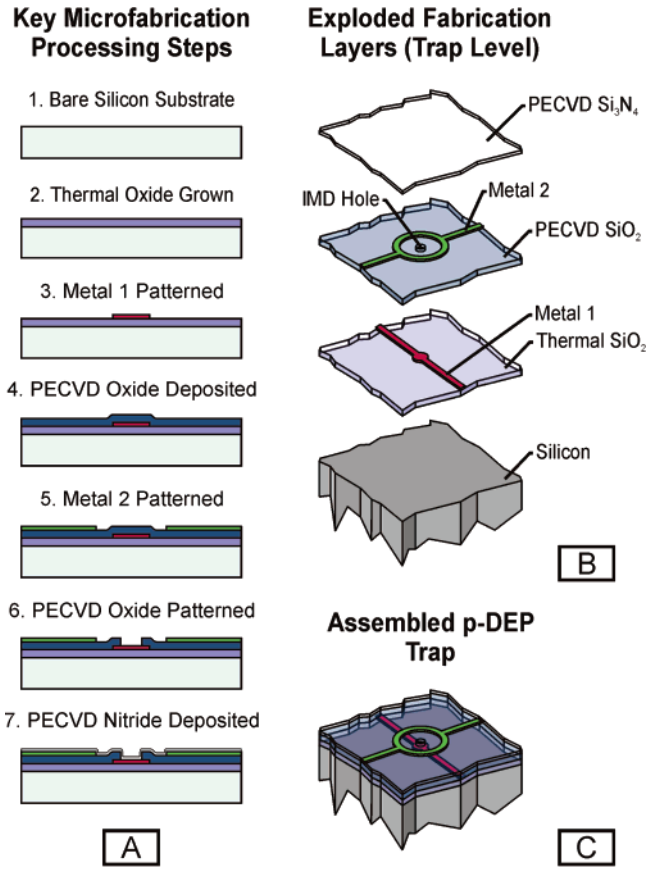

Figure 2. (A) Basic processing steps required for device fabrication. (B) and (C) provide exploded and assembled pictorial images of the distinct material layers in a single DEP trap.

wet thermal oxidation step established a grown 1.5-μm-thick silicon dioxide layer (Figure 2A-2) on ~7−25 Ω·cm phosphorus-doped 150-mm n-type wafers (WaferNet, Inc., San Jose, CA) (Figure 2A-1). We then sputter-deposited a 5000-Å-thick aluminum metallization layer (M1) onto the grown oxide, which we subsequently dry etched using BCL_3 and Cl_2 plasma-enhanced chemistries (Figure 2A-3). To provide the requisite electrical isolation between the two metal levels, we deposited a 1.5-μm-thick PECVD intermetal dielectric SiO_2 layer over the patterned M1 electrode features (Figure 2A-4). Following the same protocols prescribed for the M1 level, we sputter deposited and patterned the second and final 5000-Å-thick aluminum metallization layer (M2) (Figure 2A-5). A two-step etch process established vias in the PECVD oxide layer enabling electric field communication between the two metal layers (Figure 2A-6). The first part of the etch used an HC_{23} and oxygen-based plasma to remove the bulk of the patterned oxide regions, while the second part incorporated a timed wet etch in Silox Vapox III (Transene Co., Inc., Danvers, MA) to break through to the underlying M1 level. We parsed the wafer into individual chips using a die saw. For chips used in HL-60 cell experiments, we deposited an additional 250-Å-thick PECVD silicon nitride layer on their exposed top surfaces (Figure 2A-7). To avoid depositing this nitride layer over the bond pads, we covered them with pieces of glass coverslip prior to deposition. The nitride layer prevented direct contact between the aluminum electrodes and the cell membranes thereby preventing nonspecific adhesion of cells. Figure 2B-C displays the different layers in exploded and assembled forms of an individual DEP trap.

Device Packaging. Figure 3A presents an exploded diagram detailing the hardware used for packaging the active coverslips and enabling connections to off-chip fluidic and electrical systems. To house the devices in this assembly, we first created on-chip inlet and outlet fluidic ports by drilling two separate 0.75-mm-diameter holes in designated locations on each die. A razor-cut and awl-punched sample of double-sided tape (3M VBH 4932, St. Paul, MN) attached the chips to underlying custom-designed printed circuit boards (PCBs) (ExpressPCB, Santa Barbara, CA).

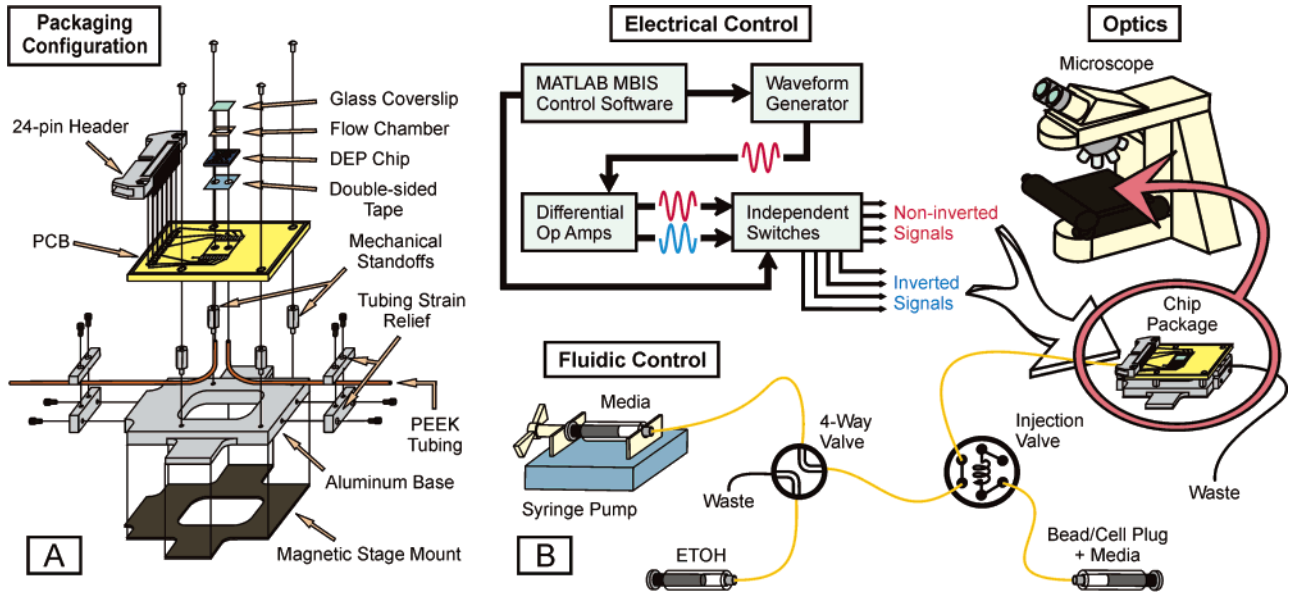

Figure 3. (A) Exploded diagram of the active coverslip packaging scheme. The test setup requires the coordination of separate electrical, fluidic, and optical control systems as outlined in (B). The electrical system (B, upper left) delivers buffered and inverted sinusoidal waveforms to the distinct row and column electrodes on the active coverslips. Using a MATLAB interface, the frequency, amplitude, and activation state of the DEP traps in the array are remotely controlled. The fluidic system (B, lower portion) delivers microparticles to our chip and the optical system (B, upper right) enables visualization of all traps during device operation.

The awl-punched holes positioned directly beneath the drilled holes in the attached chips enabled connections to the PEEK tubing (Upchurch Scientific, Inc., Oak Harbor, WA) that we press fit into to the underside of the PCBs. We assembled 3-mm-wide flow chambers with ceiling heights of 250 μm by plasma bonding custom-designed laser-cut silicone rubber gaskets (Grace Bio-Labs, Inc., Bend, OR) to 9 mm $\times$ 9 mm Bellco glass coverslips (Electron Microscopy Sciences, Ft. Washington, PA) and then affixing them to the exposed top surfaces of the mounted chips using high-performance epoxy (Loctite Fixmaster, Rocky Hill, CT). To make electrical connections between the PCB traces and the on-chip pads, we soldered fine-gauge wires to the PCBs and then linked the free ends to the chip using conductive epoxy (ITW Chemtronics, Kennesaw, GA). Prior to device testing, we protected and sealed all fluidic seams, including the backside PCB/PEEK tubing interfaces, using high-performance epoxy. We mounted the PCBs on custom-machined aluminum bases that served as mechanical supports and as a means for providing stress relief for the fluidic tubing connections during chip operation. The packaged assemblies mounted onto a steel microscope stage and remained fixed in place by means of Adhes-A-MAG magnetic sheets (Magnetic Specialty, Inc., Marietta, OH) attached to the undersides of the aluminum fixtures. A pair of finlike extensions machined into the aluminum bases allowed for additional stabilization on the stage by presenting handles for taping the assembly in place. Electrical connections to off-chip control circuitry used a 24-pin (3M 3627−5002) header connected directly into the PCB.

Electrical Control. We selectively activated on-chip row and column electrodes using a simple custom-fabricated control board. The board, operated remotely through a MATLAB-controlled PCI interface, incorporated sets of AD8132 op amps (Analog Devices, Inc., Norwood, MA), configured for single-ended input and differential output, producing phase-matched inverted and non-inverted versions of a sinusoidal input that we ported to banks of ADG333 independently selectable analog switches (Analog Devices). To electrically control a trap's holding characteristics on a given device, we set the associated M1 row electrode either to ground or to a sinusoidal voltage while simultaneously setting the associated M2 column electrode to ground or to an inverted sinusoidal input. Driving the traps in this manner establishes a difference waveform between the M1 and M2 levels that for all cases is either sinusoidal or zero. We will denote all references to the voltage applied to a given DEP trap by noting the peak voltage difference between the two electrodes. The upper left-hand portion of Figure 3B details the specifics of the electronics.

Fluidic Control. Fluidic control for introducing microparticles to the DEP trapping arrays involved a KD Scientific 210C syringe pump (KD Scientific, Inc., Holliston, MA), a series of Hamilton gastight glass syringes (Hamilton Co., Reno, NV), PEEK tubing (Upchurch Scientific), a four-way valve (Upchurch Scientific V-101D), and a six-port injection valve (Upchurch Scientific V-541), as we illustrate in the lower portion of Figure 3B. During assays, we loaded the stock solution or media needed for a given experiment into a syringe controlled by a dedicated syringe pump. The outlet from this syringe along with a separate nondriven syringe containing 70% ethyl alcohol (EtOH) (Pharmco Products, Inc., Brookfield, CT) in deionized water fed into the four-way valve. The outlet stream from the four-way valve then connected to the inlet of the six-port injection valve. Using a small 250-μL syringe, we loaded microparticles, suspended in a solution matching that found in the pump-controlled syringe, into a 19.6-μL PEEK sample loop in the injection valve. The protocol we used for microparticle injection in all experiments involved the sequential flushing of the system with EtOH, followed by a replacement with media, a bead- or cell-doped injection, and a return to operation using media.

Optics. We visualized the device using an LD Epiplan 10$\times$ objective (Zeiss, Thornwood, NY) mounted on an upright Zeiss Axioplan 2 imaging microscope. Fluorescence-based assays used an EXFO X-Cite 120 fluorescent source (EXFO Photonic Solutions, Inc., Richardson, TX) and Chroma 41001 FITC and 41007a Cy3 filter sets (Chroma Technology Corp., Rockingham, VT). We recorded all images and videos using a LaVision Imager 3 QE CCD Digital Camera (LaVision GmbH, Goettingen, Germany). The upper right-hand portion of Figure 3B highlights the optical system showing its operation in the context of the overall test platform.

Modeling. Using the electroquasistatic approximation in FEMLAB (Comsol, Inc., Burlington, MA), we modeled electric fields for various electrode configurations and ported the simulation results to an updated version of our previously developed MATLAB (The MathWorks, Inc., Natick, MA) modeling software.[51] Within the MATLAB software, we determined total system forces including multipolar DEP forces, gravitational forces, and flow-induced drag, which ultimately served to asses the holding characteristics of our designs.

For all simulations we subjected the traps to an applied 1−2-V peak potential difference delivered at frequencies ranging from 1 to 10 MHz. We set the silicon substrate's conductivity to 4×10^{-4} S/m and its relative permittivity to 11.8. Simulated oxide layers used conductivities of 1×10^{-18} S/m and relative permittivities of 3.9. We treated the system electrodes as boundaries with infinitesimal thicknesses and defined voltage conditions. All simulations used 20-μm-diameter cells with cytoplasmic conductivities of 0.75 S/m, densities of 1071 kg/m^3, and relative permittivities of 75 positioned in media possessing a conductivity of 0.1 S/m, a density of 1000 kg/m^3, and a relative permittivity of 80. We set cell membrane thicknesses to 1×10^{-9} m, membrane conductivities to 22×10^{-3} S/cm^2, and membrane capacitances to 1.6×10^{-6} F/cm^2.

Bead Experiments. The initial assays assessing the functionality of our device's row/column trap addressing scheme used commercially available 20-μm-diameter polystyrene beads coated with external silver shells (microParticles GmbH, Berlin, Germany) as model test particles. The metal coating ensured p-DEP trapping behavior, while the polystyrene core kept the overall particle density close to that of water. We ran bead experiments using media composed of a 50% w/v sucrose/deionized water solution supplemented with 1% w/v bovine serum albumin fraction V (Roche, Basel, Switzerland) and 1% v/v Triton X-100 surfactant (Sigma-Aldrich Co., St. Louis, MO) resulting in a conductivity of ~0.01 S/m. While loading the arrays, we set all row and column electrodes to an "on" state, delivering a 2-V peak potential difference cycled at 1 MHz across every trap. Using flow rates ranging from 10 to ~50 μL/min we injected bead-free media onto

(51) Voldman, J.; Braff, R. A.; Toner, M.; Gray, M. L.; Schmidt, M. A. *Biophys. J.* **2001**, *80*, 531−541.

the active coverslip arrays clearing away extraneous beads not captured in activated traps. We performed release operations for specific captured particles by grounding the row and column electrodes associated with selected traps within the arrays and then increasing the fluid flow rate.

Cell Culture. We maintained HL-60 cells (ATCC CCL-240, Manassas, VA) at 37 °C under a humidified 7.5% CO_2 atmosphere. The culture medium was RPMI 1640 (Gibco, Grand Island, NY) supplemented with 10% v/v bovine calf serum (Hyclone, Logan, UT) 1% v/v L-glutamine taken from 200 mM stock (Gibco), 100 units/mL penicillin (Gibco), and 100 μg/mL streptomycin (Gibco). We stained cells using either CellTracker Green CMFDA or CellTracker Orange CMTMR (Molecular Probes, Eugene, OR) prepared in 10 mM working solutions in dimethyl sulfoxide (DMSO) (Sigma-Aldrich) that we diluted to final concentrations of 5 μM using serum-free culture media. Immediately preceding introduction onto the chips, we rinsed the HL-60s 1−3× and suspended them at concentrations ranging from 6.5×10^5 to ~1×10^7 cells/mL in 10.25% w/v sucrose/deionized water media with electrical conductivity of ~0.01 S/m.

Cell Experiments. During cell injections we applied a 2-V, 1-MHz signal across all traps in our active coverslip devices. As in the bead assays, we released held cells by grounding the row and column electrodes tied to selected traps while simultaneously increasing the fluid flow. The 10 to ~50 μL/min injection rates again proved useful for ensuring single-cell loading in the trap arrays. In contrast to the bead-based studies, we replaced a standard system syringe with another containing trypsin−EDTA (1×) (Gibco) and ended all cell assays by flushing the chips with this enzymatic cleaving agent. Through this step and the subsequent EtOH flush and N_2 drying procedures, we sought to minimize device fouling and enable multiple experiments with a given chip. To enhance cell viability we heated all solutions to 37 °C in a controlled water bath immediately prior to plumbing them into the fluidic control system.

Safety Considerations. Our microfabrication sequence demanded the use of numerous chemicals possessing varying levels of reactivity, flammability, and toxicity. The M1 and M2 aluminum etch processes involved chlorine-based chemistries that serve as strongly corrosive oxiders promoting irritations to the skin, eyes, and mucous membranes upon exposure. The Silox Vapox III silicon dioxide etchant contains significant concentrations of ammonium fluoride. In a delayed response after exposure, this component produces severe and potentially life-threatening burns via bone degradation and therefore demands extreme caution and proper personal protective equipment. Piranha cleaning processes incorporated early on in device fabrication presented avenues for exposure to heated sulfuric and hydrogen peroxide mixtures. Photoresists, used to pattern features in different levels of the device architectures, promote sterility for some women upon continued exposure. On the device operations side, cell staining solutions contain the poison DMSO. Ingesting this toxin can severely irritate the respiratory tract.

RESULTS AND DISCUSSION

Our active coverslip technology involves the integrated coordination of a fluidic microparticle delivery system, optical scanning and visualization tools and an electrically activated addressable array of p-DEP cell traps. Below we describe the development and functionality of the system's p-DEP traps and the trap-specific release capabilities afforded by our row/column addressing architecture.

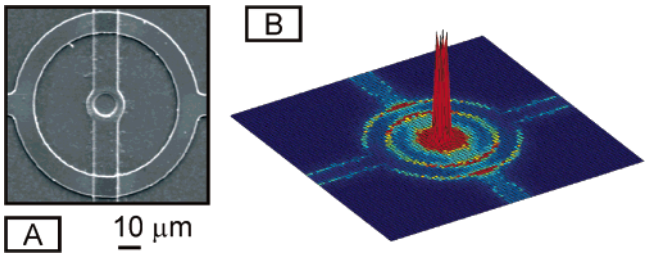

Figure 4. Ring-dot trap design. (A) shows an SEM of a completed trap, while (B) demonstrates high-strength localized DEP holding characteristics by plotting the square of the magnitude of the electric field in a horizontal plane positioned 1 μm above the electrode surface.

Trap Design and Development. The "ring-dot"-shaped traps (see Figure 4A) in our active coverslip devices enable the holding of individual microparticles in defined locations. We developed this design using an iterative process where we assessed DEP holding characteristics for a series of different electrode configurations (data not shown). The final ring-dot design presents a high-strength spatially localized trap well-suited for integration into our microparticle trapping arrays (see Figure 4B).

Varying the radius of the inner "dot" of the ring-dot structures, changing the distance between the trap electrodes, or both offers avenues for tuning the holding response of a given implementation. For all of the ring-dot trap designs that we modeled and tested, the simulated DEP holding forces localized to the dot region in each trap ranged between 240 and 430 pN when subjected to 2 V at 1 MHz. This trapping strength was more than enough to stably hold both beads and HL-60 cells when subjected to volumetric flow rates on the order of 10 to ~50 μL/min.

We should point out that the ring-dot trap design inherently requires p-DEP operation. If either the conductivity of the media or the drive frequency of the electrodes creates n-DEP forces, the dot features in each trap will actively push microparticles out of the array. Since it is straightforward to obtain p-DEP trapping with most cell populations, this requirement is not a strong limitation. While operating only in the p-DEP domain might restrict our ability to selectively trap cells (based upon their electrical properties), this consequence is not a limitation in our case since our device is expressly designed to trap all types of cells; we do not want the electrical trapping to be specific or preferential to any distinct subset of cells.

In the context of our active coverslip device application, the ring-dot design shows several advantages over existing DEP trap geometries. Because we arrange both the M1 and M2 electrodes in a planar format and in proximity to one another, we avoid the flow chamber height restrictions encountered by other DEP trapping arrays.[39,49] Specifically, we are not required to position the flow chamber ceiling and the trapping array substrate close to one another to ensure strong electric field communication between the two facing surfaces. Lifting this restriction sidesteps any need for precision alignment when bonding the flow chamber to the top surface of our devices. The independent placement of the substrate and flow chamber ceiling further permits increased chamber heights, allowing higher flow rates during assays. Higher flow rates ultimately lead to more rapid sorting. Last, the ring-

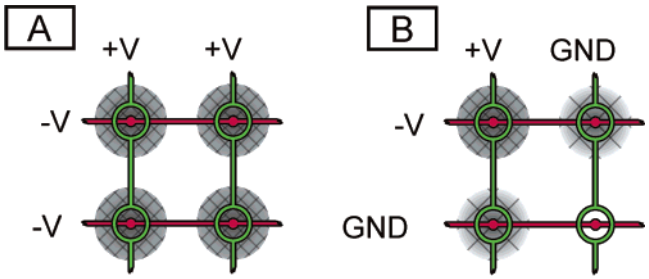

Figure 5. Illustration of the scalable passive row/column trap addressing scheme. (A) shows a 2 × 2 array where all traps are in the "on" state (dark gray highlights). (B) indicates the same array with the lower right trap set to the "off" state (no gray highlights). This condition is realized by grounding the associated row and column electrodes. Traps on the same row and column are "on" but activated in a quarter-strength configuration (midtone gray highlights).

dot designs demonstrate geometrical symmetry, presenting a trapping field capable of loading microparticles regardless of the flow direction used for their introduction. Although flow direction is not especially important for our devices, other applications could potentially benefit from the flexibility presented by this symmetry.

Novel Scalable Addressing Architecture. Figure 5 highlights the row/column array architecture used for addressable release operations on our active coverslips. Rather than routing individual sets of electrodes to each of the DEP traps positioned in the arrays,[30,50] we used two separate metal levels to tie all traps to row- (M1) and column-based (M2) electrodes. During testing, we realized trap-specific release operations by grounding the row and column electrodes associated with individual traps positioned within the array. Using such a scheme deactivates the DEP holding forces acting on the lone trap positioned at the intersection of the grounded row and column electrodes (lower right in Figure 5B). Subsequent ramping of the suspension media flow rate removes the released microparticle from the trapping array, enabling downstream collection and further study. Aside from deactivating the traps positioned at the intersection of grounded row and column electrodes, our selection scheme forces all other traps in grounded rows and columns into "quarter-strength" states where the peak voltage difference between the two metal levels in a given trap is half that of a normal "on" state trap (upper right and lower left in Figure 5B) and the DEP holding strength is one-fourth of its original "on" state value. By balancing the holding characteristics of these quarter-strength traps with the flow rate, we can ensure that release operations occur solely at the grounded electrode intersections.

Trapping and Sorting of Beads and Cells. In our first proof-of-concept device implementation, we tested a simple 4 × 4 DEP array of our ring-dot traps. This design was large enough to functionally demonstrate the addressable selection of specific traps and test the ability for quarter-strength traps to retain their held microparticles while avoiding the unnecessary overhead associated with larger formats.

We observed ideal array loading behaviors, where individual microparticles positioned themselves directly over the high-field central dot locations in each of the traps, throughout numerous experimental runs, examined on separate days, using both silver-coated test beads and HL-60 cells. This prevalent single-microparticle capture response resulted largely from the localized DEP fields associated with our ring-dot trap design. In cases where microparticles from the flow field impinged upon beads or cells

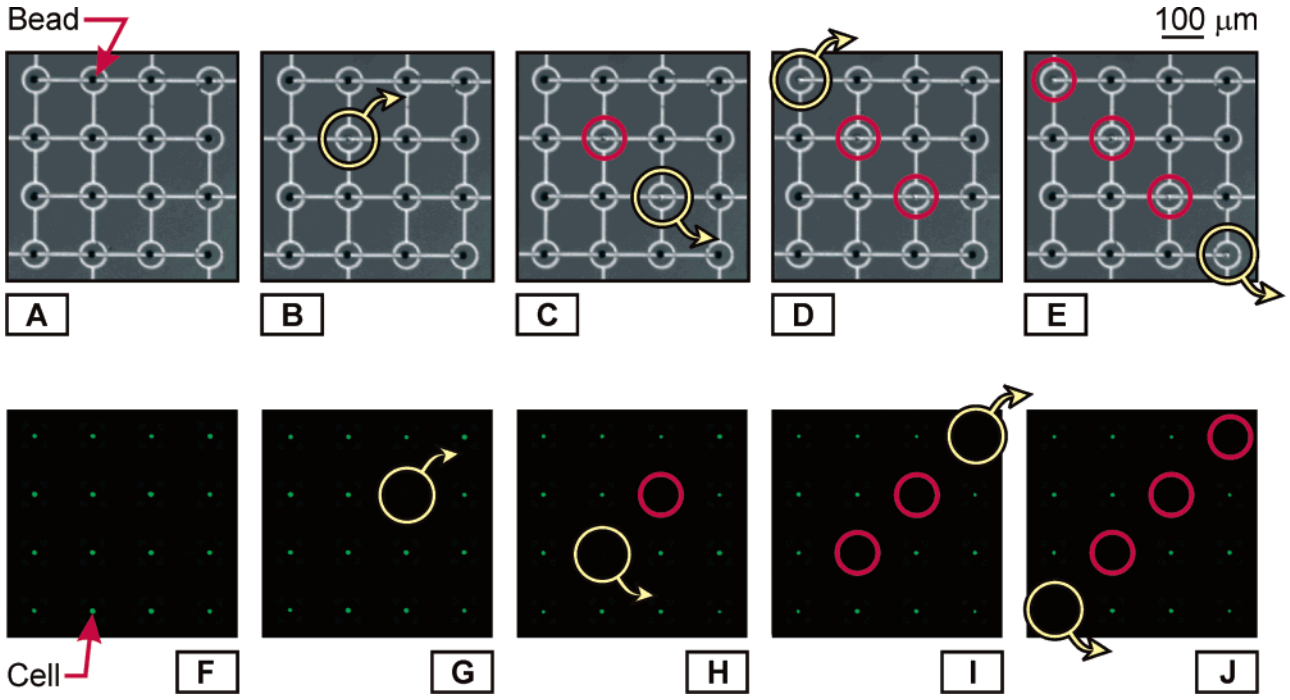

Figure 6. Two separate sets of images detailing the sequential row/column-based release routines used to produce diagonals of empty traps in 4 × 4 p-DEP arrays. (A–E) detail manipulations of 20-μm-diameter silver-coated beads while (F–J) outline operations with HL-60s. In both (A) and (F), each of the 16 traps is filled with a single microparticle. This condition is the starting point for all sorting assays. Red circles highlight locations where microparticles have been released while yellow circles with attached arrows indicate the specific traps where sorting is occurring in a given frame. Further removal of additional trapped microparticles beyond the states shown in (E) and (J) simply requires subsequent additional row/column trap deactivation steps. Though not shown here, in all bead and cell release assays microparticles were sequentially removed piecewise until the arrays were emptied.

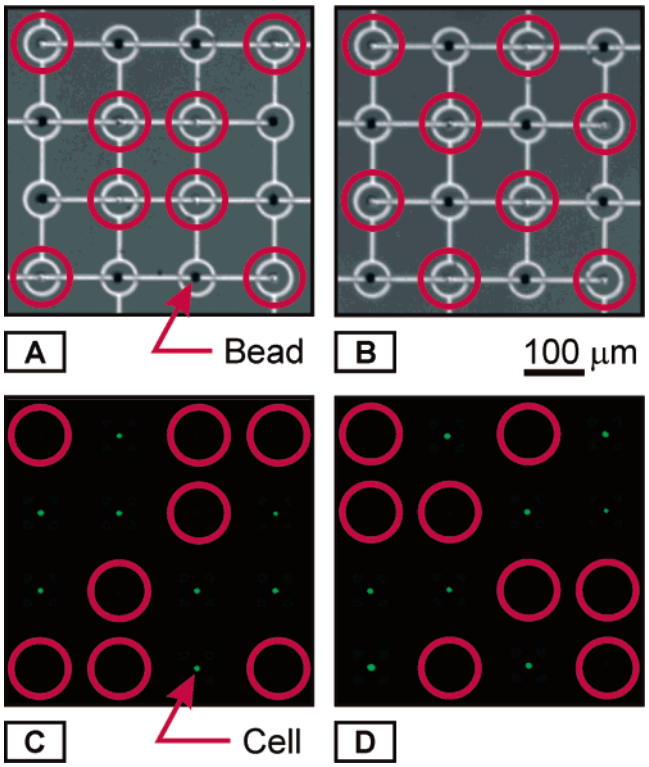

Figure 7. Additional array functionality. Here we show two unique bead-based removal configurations (A, B) and separate fluorescence microscopy images showing sorting of trapped HL-60 cells in a 4 × 4 array (C, D). In all cases, red circles indicate locations where beads or cells have been removed from the trapped populations.

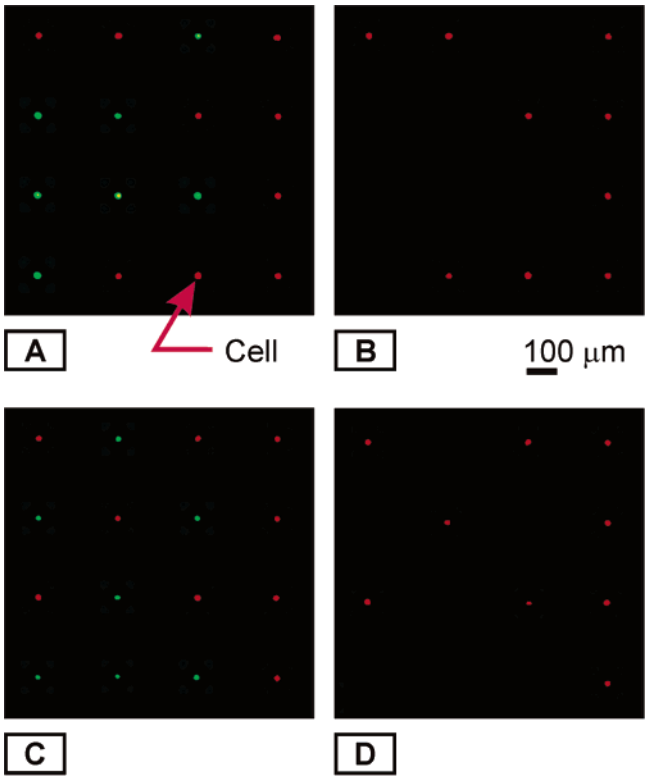

Figure 8. Image-based cell sorting. (A) and (C) show images from two assays where mixtures of orange and green CellTracker-stained HL-60 cells are loaded into a 4 × 4 array. Though the initial placement of the green and orange cells is random in nature, the addressable traps enable selective sorting for all cells of a prescribed color in both (B) and (D).

already captured in the 16-trap arrays, hydrodynamic drag forces dominated over the DEP capture potential thereby preventing the accumulation of multiple microparticles in individual traps (see Supporting Information video 1). Beyond witnessing this single-microparticle capture response, we generally did not observe the nonspecific attachment of test beads or cells to the exposed surfaces of the active coverslip chips. Figure 6A and Figure 6F highlight this desired loading condition for beads and cells, respectively, in two separate 4 × 4 arrays.

To demonstrate the trap-specific addressing capabilities of our design, we conducted numerous experiments sequentially removing microparticles from fully loaded 16-trap arrays and reducing them, one microparticle at a time, to empty trapping structures. Figure 6 highlights several of the initial extractions made during two separate examples of this sort of sequential release assay. Each image highlights one step along the path pursued in producing an empty array. Supporting Information video 2 provides a real-time visual of this addressing scheme in action. The video shows extractions of the center four beads from an initially fully loaded 16-trap array.

Although we did not optimize our geometries to minimize sorting time, the time necessary for releasing trapped microparticles was in the range of seconds. We first released cells using a slow-flow rate (~μL/min). Once the released microparticle moved downstream beyond the outer "ring" of a given trap, we reactivated all row and column electrodes in the system and increased the flow rate (tens of microliters per minute) to rapidly remove the designated microparticle from the trap array. Each step in this two-part process requires only a few seconds.

We present higher level functionalities for our array technology in Figure 7. Panels A−D in Figure 7 provide four distinct examples of complex and symmetric release patterns that further validate our addressing strategy. Forming such prescribed patterns would have been impossible with a nonfunctional row/column trap selection scheme. Our active coverslip devices operated effectively for both test beads as well as for our examined HL-60 cell line.

Finally, we demonstrate our ability to successfully sort imaged cell populations in Figure 8. Figure 8A and Figure 8C show two different assays where mixtures of green and orange fluorescently stained HL-60s are loaded into a 4 × 4 array. The arrangement of the green and orange cells in each experiment is randomly established by the relative concentrations of the two different cell types in the injection plug and their subsequent chance encounters with any one of the DEP traps in the array. After loading, we are able to image the cells using multicolor fluorescence microscopy and then sort out any desired subpopulation based upon the fluorescence signal. Because we have little control over the loading pattern that develops during a given assay, the selective removal of all of the cells of a specific color as shown in Figure 8B and Figure 8D conclusively demonstrates the operation of our row/column-based architecture for trapping, imaging, and then sorting individual cells.

On the whole, our technology offers several key advantages when compared to prior microparticle manipulation systems. The row/column electrode format bypasses any need for integrating transistor elements directly into the device substrate, avoiding the microfabrication complexities seen in prior small-scale addressable

arrays.[49] Furthermore, the architecture does not pose a limitation on the permissible packing density of traps positioned in the capture arrays, as would likely be the case if individual, isolated electrodes controlled the activation state of each trap.[30,50] Interconnect demands for our row/column architecture scale as $2\sqrt{n}$, where n represents the number of traps in a given array possessing equal numbers of rows and columns. To illustrate this advantage, scaling our technology to larger designs capable of controlling 10 000 individual traps would demand 200 chip-to-world electrical ties in contrast to the potential need for 10 000 electrical connections when handled through separate trap-specific electrodes. Packaging an array scaled to this extent presents manageable requirements for currently available automated wire-bonding and chip-packaging technologies. In many cases, the number of traps positioned within an array directly influences the array's suitability for a given application. Our new trapping architecture, which now allows scaling to large numbers of traps, will be useful for screens that require imaging and then sorting of large populations of cells.

CONCLUSIONS

We have presented an active coverslip technology that demonstrates the first known implementation of a scalable, transistor-independent, p-DEP-based architecture for sorting captured microparticles from a surveyed population. The unique planar p-DEP traps arranged into our row/column electrically connected topologies show strong highly spatially localized holding characteristics. Using an illustrative 4×4 array, we effectively demonstrated the functionality of our unique addressing strategy with both test beads and mammalian cells. This new architecture now enables the efficient addressing of thousands of DEP traps for cell-sorting applications.

ACKNOWLEDGMENT

This work was supported by the NIH (RR19652) and NSF Graduate Fellowship funding. We thank Anderson Nnewihe for developing the control circuitry. We also thank the Microsystems Technology Laboratories and the Edgerton Center Student Shop at MIT for technical advisement and facilities access.

SUPPORTING INFORMATION AVAILABLE

Two AVI videos demonstrating (1) the single-cell capture capabilities of our "ring-dot" trap geometry and (2) the selective removal of the center four beads in a fully loaded 16-trap DEP array. This material is available free of charge via the Internet at http://pubs.acs.org.

Received for review July 30, 2005. Accepted October 19, 2005.

AC0513616